Current Research in Food Science 4 (2021) 215–223

Contents lists available at ScienceDirect

Current Research in Food Science

journal homepage: www.editorialmanager.com/crfs/

Research Paper

Encapsulation and controlled release of vitamin C in modified cellulose nanocrystal/chitosan nanocapsules

Jiyoo Baek [a], Mohankandhasamy Ramasamy [a], Natasha Carly Willis [b], Dae Sung Kim [a], William A. Anderson [a], Kam C. Tam [a,*]

[a] Department of Chemical Engineering, Waterloo Institute for Nanotechnology, University of Waterloo, 200 University Avenue, Waterloo, ON N2L 3G1, Canada
[b] Department of System and Design Engineering, Waterloo Institute for Nanotechnology, University of Waterloo, 200 University Avenue, Waterloo, ON N2L 3G1, Canada

ARTICLE INFO

Keywords:
Vitamin C (L-ascorbic acid)
Cellulose nanocrystal
Chitosan
Nanocapsule
Antioxidants
Functional foods

ABSTRACT

Vitamin C (VC), widely used in food, pharmaceutical and cosmetic products, is susceptible to degradation, and new formulations are necessary to maintain its stability. To address this challenge, VC encapsulation was achieved via electrostatic interaction with glycidyltrimethylammonium chloride (GTMAC)-chitosan (GCh) followed by cross-linking with phosphorylated-cellulose nanocrystals (PCNC) to form VC-GCh-PCNC nanocapsules. The particle size, surface charge, degradation, encapsulation efficiency, cumulative release, free-radical scavenging assay, and antibacterial test were quantified. Additionally, a simulated human gastrointestinal environment was used to assess the efficacy of the encapsulated VC under physiological conditions. Both VC loaded, GCh-PCNC, and GCh-Sodium tripolyphosphate (TPP) nanocapsules were spherical with a diameter of 450 ± 8 and 428 ± 6 nm respectively. VC-GCh-PCNC displayed a higher encapsulation efficiency of 90.3 ± 0.42% and a sustained release over 14 days. The release profiles were fitted to the first-order and Higuchi kinetic models with R^2 values greater than 0.95. VC-GCh-PCNC possessed broad-spectrum antibacterial activity with a minimum inhibition concentration (MIC) of 8–16 μg/mL. These results highlight that modified CNC-based nano-formulations can preserve, protect and control the release of active compounds with improved antioxidant and antibacterial properties for food and nutraceutical applications.

1. Introduction

Vitamin C (VC), commonly known as L-ascorbic acid, is a water-soluble vitamin that helps construct the biological systems via various physiological functions, such as hydroxylation reactions in collagen synthesis, growth and repair of skin, and connective tissues (Bendich et al., 1986; Naidu, 2003; Sauberlich, 1994). VC is an antioxidant necessary to prevent damage to essential macromolecules in the body by scavenging harmful free radicals caused by environmental pollution and possibly infectious organisms (Bendich et al., 1986; Bodannes and Chan, 1979). Because of its antioxidant potency, VC is quickly oxidized to dehydroascorbic acid (DHA) and hydrolyzes at alkaline pH to form an irreversible 2,3-L-diketogulonate (Simpson and Ortwerth, 2000). Therefore, encapsulating VC in nanoparticles can protect the degradation of the active compound from external environments, including light, maintaining stability and enhances the shelf-life of vitamin-based products.

Increased consumer awareness of potentially harmful synthetic preservatives and the need for biodegradable and sustainable materials has led to research into natural alternatives, notably chitosan biopolymers and cellulose nanocrystals. Chitosan (Ch) is the second most abundant natural polymer, making it ideal for biomedical and food applications (Akhlaghi et al., 2015; Kumar, 2000). Because of its mucoadhesive characteristics, the Ch delivery system can transport bioactive agents with a longer residence time in the gastrointestinal tract with improved bioavailability (Jiménez-Fernández et al., 2014). In an acidic environment, Ch protonates and bind efficiently to anionic compounds (Rinaudo, 2006; Wang et al., 2017). However, Ch has low solubility above the pH of 6.5, which limits its application. Therefore, it is imperative to modify Ch for extended applications over a wide pH range.

There are several reports on the synthesis of water-soluble Ch-compounds (Lim and Hudson, 2003; Liu et al., 2011), and modifying Ch with quaternary ammonium groups has been shown to significantly improve

Abbreviations: VC, Vitamin C; CNC, Cellulose nanocrystals; PCNC, Phosphorylated-CNC; TPP, Sodium tripolyphosphate; GCh, GTMAC-Chitosan; VC-GCh-PCNC, Vitamin C-GTMAC-Chitosan with Phosphorylated-CNC; VC-GCh-TPP, Vitamin C-GTMAC-Chitosan with Sodium tripolyphosphate.

* Corresponding author.
E-mail address: mkctam@uwaterloo.ca (K.C. Tam).

https://doi.org/10.1016/j.crfs.2021.03.010
Received 9 January 2021; Received in revised form 22 March 2021; Accepted 28 March 2021

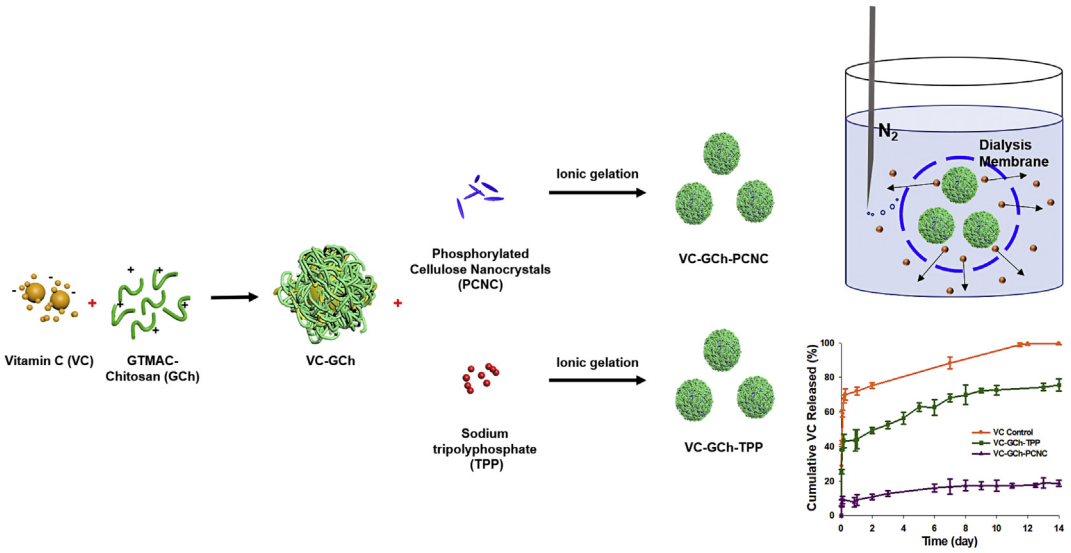

Scheme 1. Schematic illustration describing the formation of VC-GCh-TPP and VC-GCh-PCNC nanocapsules by utilizing VC, GCh, TPP, and PCNC.

the aqueous solubility of Ch. Moreover, the GTMAC could be conjugated to Ch by reacting with the epoxide rings yielding a cationic GCh that could electrostatically bind to VC due to the presence of quaternary ammonium groups. Furthermore, GTMAC has been shown to possess better antimicrobial properties, which could preserve the nanocapsules and VC from degradation (He et al., 2018). Henceforth, glycidyl trimethylammonium chloride (GTMAC) was conjugated to Ch to enhance the solubility, attachment and preserve the negatively charged VC.

Cellulose nanocrystal (CNC) is extracted via sulfuric acid hydrolysis to produce sulphated-CNC (SCNC). However, such a system may not be suitable for biomedical or food applications since sulphated materials are rarely used as food acidulants. On the other hand, phosphoric acid is considered the most common inorganic food acidulant (Deshpande, 2002), and a safer and healthier hydrolyzing acid for functionalizing CNC. Therefore, cellulose fibres were hydrolyzed using phosphoric acid to isolate the crystalline regions of phosphorylated-cellulose nanocrystals (PCNC) (Espinosa et al., 2013; Vanderfleet et al., 2018).

Sodium tripolyphosphate (TPP) is often used as a cross-linking agent to prepare chitosan-TPP complexes. These complexes are metastable, as well as having low mechanical strength, and therefore, they have limited applications as delivery systems (Alishahi et al., 2011; de Britto et al., 2012; Katouzian and Jafari, 2016). To address this shortcoming, PCNC was adopted as a novel cross-linking agent for GCh to produce VC encapsulated nanocapsules (VC-GCh-PCNC) via ionic gelation. Wang et al. (2017) used both TPP and SCNCs as cross-linking agents to encapsulate hydrophilic anthocyanins. They confirmed that chitosan-SCNCs yielded more stable capsules, where the external pH modulated the active molecule release (Wang et al., 2017).

Desai and Park also showed that TPP cross-linked chitosan microspheres displayed almost 100% cumulative VC release in approximately 6 h (Desai and Park, 2005). A better carrier system with a higher encapsulation efficiency and sustained release rate, which also shields the active ingredients (such as VC) from degradation (Ashrafizadeh et al., 2020) is needed. Ideally, GCh-PCNC nanocapsules could provide a better encapsulation, prolonged-release rate and enhanced stability than existing carrier systems.

Based on this rationale, the present study seeks to produce a better carrier system with a higher encapsulation efficiency and sustained release of VC using GCh-PCNC nanocomplex. The VC nanocapsule characteristics, such as particle size, degradation, encapsulation efficiency, cumulative release, simulated release, and release kinetics, were analyzed and elucidated. Additionally, we investigated the nanocapsule's antioxidant activity and antibacterial characteristics.

2. Materials and methods

2.1. Materials

Vitamin C (L-ascorbic acid), low to medium molecular weight chitosan (M_w = 50–190 kDa), phosphoric acid, glycidyl trimethylammonium chloride, acetic acid, sodium acetate trihydrate, PBS buffer, hydrochloric acid, and sodium hydroxide were purchased from Sigma-Aldrich (St. Louis, MO, U.S.A.) and used as received.

2.2. Preparation of VC-GCh-PCNC/VC-GCh-TPP nanocapsules

PCNC and GCh were prepared based on the previously reported protocol with minor modifications (Baek et al., 2019). Initially, suspensions of GCh (2 mg/mL) and PCNC (4 mg/mL) and a solution of TPP (0.9 mg/mL) were prepared in Milli-Q water. The concentrations of TPP and PCNC were selected based on the phosphate ion concentrations. GCh and PCNC suspensions were sonicated in a light-protected environment for 10 min (Misonix Sonicator XL-2000 Series, QSonica LLC) to produce a stable dispersion. Under nitrogen purging, 0.5 mL of VC solution was added to 10 mL of GCh, and the suspension was ultra-sonicated for 5 min. A 2 mL of PCNC or TPP was added using a Harvard Apparatus syringe pump into the VC-GCh dispersion every 50 s with continuous ultra-sonication to obtain VC-GCh-PCNC/VC-GCh-TPP nanocapsules as shown in Scheme 1. The prepared samples were stored in the dark at 4 °C and subsequently utilized for further evaluation.

2.3. Characterization

2.3.1. FTIR

TPP and PCNC were analyzed using the FTIR spectrophotometer (Bruker Tensor 27 FTIR spectrometer, Billerica, MA, USA) to confirm the presence of phosphate groups. Freeze-dried samples were ground in a mortar and compressed with potassium bromide (KBr) to form pellets. FTIR spectra of each sample were recorded between 4000 cm^{-1} and 400 cm^{-1} with a resolution of 4 cm^{-1} and 32 scans.

2.3.2. Characterization of the nanocapsules

The particle size and zeta potential of VC-GCh, VC-GCh-PCNC and VC-GCh-TPP were determined using a Malvern Zetasizer Nano ZS instrument (Nanosizer ZS, Malvern, UK). All the experiments were carried out in triplicate.

2.3.3. Morphology

The morphology of SNPs was evaluated using a transmission electron microscope (TEM, Philips CM10 electron microscope, an acceleration voltage of 60 kV). The sample was placed on a 200-mesh carbon-coated copper grid and air-dried before analysis.

2.4. Degradation analysis of VC

Degradation reaction upon storage or processing is the main problem of nutritional quality loss. To determine the optimal conditions required for further experimental studies, the degradation of VC at normal and controlled conditions were conducted. VC solution, equivalent to the concentration in the nanocapsules used in other studies, was prepared using the phosphate-buffered saline (PBS, pH 7.4) in a rubber-stoppered round bottom flask. Nitrogen purging and sample withdrawal were facilitated through the inlet and outlet needles. The flask was covered with aluminum foil and left to stir at 250 rpm at room temperature. For comparison, another flask with the same experimental setup was used, but without nitrogen purging and covering with the aluminum foil. At the designated time intervals, 1 mL aliquot of the solution was withdrawn and analyzed at 265 nm using a UV–Visible spectrophotometer (Cary 100 Bio UV–Vis spectrophotometer with quartz cuvettes). The concentration of VC was determined from the calibration curve.

2.5. Determination of encapsulation efficiency

An encapsulation efficiency (EE, %) was performed on VC-GCh-PCNC and VC-GCh-TPP nanocapsules. At first, 1 mL of the sample dispersion was filtered using a 25 nm pore size membrane (Durapore membrane filter PVDF 0.025 μm, Sigma-Aldrich, St. Louis, MO, U.S.A.) placed in a stainless-steel syringe filter holder (Millipore and 1 Whatman 13 mm). The VC content in the filtrate was measured using the Cary 100 Bio UV–Vis spectrophotometer. The encapsulated VC concentration was determined from the VC calibration curve and used to determine the EE from Eq. (1) (Akhlaghi et al., 2015).

$$EE(\%) = \frac{[VC]_{total} - [VC]_{filtrate}}{[VC]_{total}} \times 100\% \quad (1)$$

where VC_{total} is the absorbance of the control and $VC_{filtrate}$ is the absorbance of the unbound VC.

2.6. Cumulative VC release study

The cumulative release of VC from VC-GCh-PCNC or VC-GCh-TPP was performed based on the modified method of Desai and Park (2005). 10 mL of the nanocapsule dispersions was placed separately in a dialysis bag, submerged in 25 mL of PBS (at pH 7.4 and 25 °C) on a stirrer-plate with continuous nitrogen purging and under controlled light exposure. The dialysate was collected at predetermined time intervals (0–72 h, and up to 14 days), and the VC release was analyzed using the Cary 100 Bio UV–Vis spectrophotometer. A control test with a similar experimental condition was also performed for the VC solution. This cumulative release study was conducted in triplicate, and the average values were reported.

2.7. DPPH free radical scavenging activity

A colorimetric 2,2-diphenyl-1-picrylhydrazyl (DPPH) assay was used to measure the free radical scavenging activity of VC, VC-GCh-PCNC and VC-GCh-TPP. The method was adapted with a slight modification based on the reported assay (Wang et al., 2017). DPPH is reduced when it reacts with an antioxidant reagent, causing a colour change from violet to yellow. Initially, the DPPH solution (0.025 mg/mL) was prepared in pure methanol and protected from light using an aluminum foil. The nanocapsule suspensions were filtered through a 25 nm pore size membrane, and 0.15 mL of the filtrate was stirred with 1 mL DPPH solution in the dark for 30 min and 5 days. Finally, the absorbance was measured using the Cary 100 Bio UV–Vis spectrophotometer. The encapsulated VC concentration was determined from a standard VC calibration curve. The scavenging activity was calculated using Eq. (2):

$$SA\% = \frac{A_{control} - A_{sample}}{A_{control}} \times 100 \quad (2)$$

where $A_{control}$ is the absorbance of the control and A_{sample} is the absorbance of the free VC.

Table 1
Experimental conditions to simulate the digestive system.

Digestive Region	pH	Time (h)
Upper Stomach	5	1
Lower Stomach	2	3
Duodenum	7.4	1
Small Intestine	5	3

2.8. Drug release kinetics and mathematical models

Various types of mathematical models have been used to determine the kinetics of drug release from the delivery systems, such as zero order, first order, and Higuchi model (Starychova et al., 2014; Zandi, 2017). These dissolution models are necessary to study the release mechanism of drugs, as it mathematically describes the release profiles, such as the release of VC.

The three models are shown below (Azevedo et al., 2014; Siepmann, 2013), where M_t is the amount of active ingredient eluted at time t, M_0 is the initial amount of VC in the solution (in most of the cases, $M_0 = 0$) (Larsen et al., 2013; Rosenzweig et al., 2013).

Various kinetic release models

Zero-order equation: $M_0 - M_t = K_0 t$ (3)

First-order equation: $\log M_0 - \log M_t = K_1 t/2.303$ (4)

Higuchi equation: $M_0 - M_t = K_H t^{1/2}$ (5)

* K_0 is the zero-order release constant.
* K_1 is the first-order release constant.
* K_H is the Higuchi dissolution constant.

2.9. Digestive system simulation release test

A released study was conducted in a simulated digestive system by modifying the pH of the environment based on conditions shown in Table 1 (Li et al., 2020). To mimic the gastrointestinal tract, the pH of the system was altered by replacing the buffer solution at specified time intervals using acetic acid-sodium acetate buffers for pH 2 and 5 and a PBS buffer for pH 7.4. The release tests were performed in the dark with continuous nitrogen purging and stirring with a magnetic stirrer at the physiological temperature (37 °C).

2.10. Antibacterial tests

Escherichia coli (E. coli) and *Staphylococcus aureus* (*S. aureus)* were used as the model for Gram-negative and Gram-positive bacteria respectively. Each strain was streaked from −80 °C glycerol stock on Lauria-Bertani agar (LBA) plates and kept overnight at 37 °C. Fully grown, a single colony bacteria was inoculated in fresh LB medium in an Erlenmeyer flask and incubated on a shaking incubator (250 r/min) for 16 h at 37 °C. Phenotypic assays were performed using overnight cultures after re-inoculating bacteria in LB broth at 0.05 initial turbidity at optical density 600 nm. The effects of VC-GCh-PCNC on both bacteria were evaluated using the standard broth dilution method. In brief, different

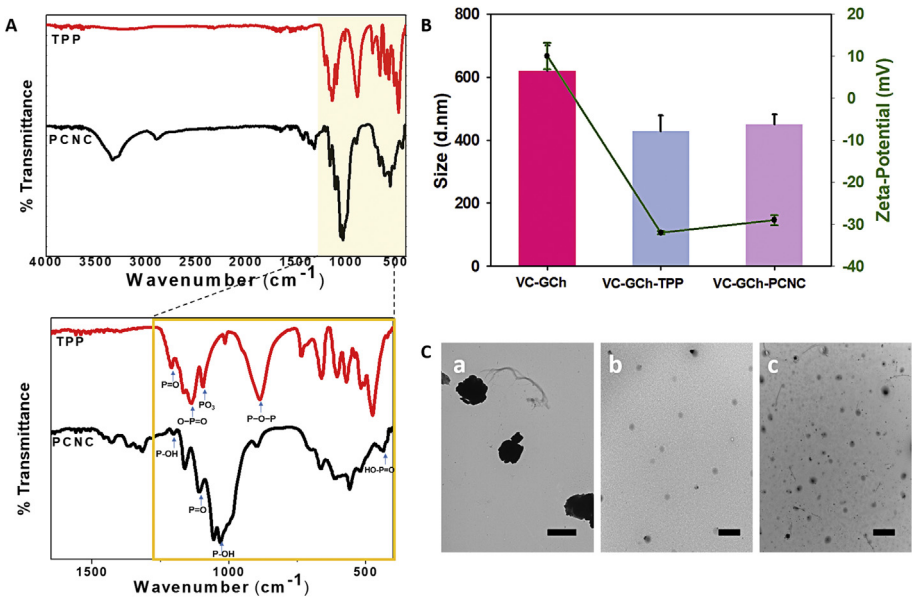

Fig. 1. (A) The IR spectra of TPP (upper trace) and P–CNC (lower trace); **(B)** Zeta potential and z-average particle sizes of VC-GCh, VC-GCh-PCNC and VC-GCh-TPP nanocapsules, and **(C)** TEM images of (a): VC-GCh complex (Scale bar: 500 nm) (b): VC-GCh-TPP (Scale bar: 2 μm), and (c): VC-GCh-PCNC (Scale bar: 2 μm).

concentrations of the dried nanoparticles (128, 64, 32, 16, 8, 4, 2, 1 μg/mL) were dispersed in sterile LB broth and sonicated. Subsequently, the turbidity of bacterial suspension (10^5 CFU/mL) was adjusted, co-inoculated and incubated in a shaking incubator for 24 h. After that, each of the bacteria-nanocapsule suspensions was serially diluted to achieve 10^8 to 10^3 CFU/mL. The samples were vortexed for 5 s, and 100 μL of the suspension was spread on the agar plate and incubated for 24 h at 37 °C. Finally, the MIC was determined according to the lowest concentration that inhibited the maximum visible growth of microbes (Shi et al., 2015).

2.11. Statistical analysis

All experiments were performed as three independent replicates, and the results are expressed as the average with error bars of ± standard deviations.

3. Results and discussion

The loading of active ingredients, such as vitamins or drugs in the nanoparticulate system can be prepared with surface charge interaction mechanisms (de Britto et al., 2012). The active ingredients, either physically entrapped (incubation) or adsorbed (incorporation) on the surface of polymer matrices to form the particles (Radtchenko et al., 2002). Polysaccharide nanoparticles (such as chitosan nanoparticle) displayed enhanced loading efficiencies, and slow/sustained release (Lazaridou et al., 2020). GCh is soluble in neutral pH medium, which ensures that the chemical degradation of the vitamin does not occur during the nanoparticle formation. The preparation, loading, and release of VC in the GCh nanocapsules will be discussed later.

The FTIR was conducted to compare the two cross-linking agents and confirm the functional groups on TPP and phosphoric acid hydrolysis for preparing the PCNC. The spectra of both TPP, PCNC are shown in Fig. 1A. The spectrum (*enlarged view*) of TPP possesses peaks at 1210-1218 cm^{-1} which are associated with the stretching vibration of P═O. The band at 1130-1156 cm^{-1} is assigned symmetrical and asymmetric stretching vibration of PO_2, and the peak at 1090-1094 cm^{-1} is attributed to the symmetrical and asymmetric stretching vibration of PO_3. The asymmetric peak presents at 888-892 cm^{-1} is a result of P–O–P stretching (Martins et al., 2012). To confirm the esterification of CNC through the phosphoric acid hydrolysis, the IR spectrum of PCNC was also determined. As was similarly found in the IR spectrum of TPP, phosphate groups were dominantly featured in the PCNC IR spectrum, revealing the presence of P–OH stretching with peaks at 1000–1034 and 1223-1236 cm^{-1}, a peak at 1164 cm^{-1} is attributed to P═O bands, and peak at between 464 and 452 cm^{-1} attributed to the HO–P═O band (Loutfy et al., 2016).

In our previous study (Baek et al., 2019), we observed that the shape of the nanocomplexes changed from a rod-like to hard-sphere and random coil morphology as the GCh/PCNC ratios were increased. This microstructure is considered to be optimal for the preparation of the VC encapsulation system (Geng et al., 2015). The negatively charged PCNC interacted with the positively charged GCh via electrostatic interaction at all pHs, resulting in the retention of VC over a prolonged period. Moreover, CNC is a strong reinforcing agent for the polymer matrix (Geng et al., 2015). Sampath et al. reported strong inter-and intramolecular interactions, resulting from hydrogen bonding between hydroxyl and amino groups on chitosan and hydroxyl groups on CNC (Sampath et al., 2017). As a result, the complexation of PCNC and chitosan significantly increased the mechanical properties of the nanocomplex. Poor mechanical strength leads to low drug loading capacity and burst release of the drug, whereas high mechanical strength produced a sustained drug release due to strong interaction between drug and matrix (Xu et al., 2020).

Lin et al. (2016) developed a double membrane hydrogel with anionic alginate, and cationic CNC (CCNC) via electrostatic interactions and the drugs were encapsulated within the membranes of the hydrogel. By adding CCNC, enhanced mechanical properties, robust hydrogel and sustained drug release were observed. This CCNC provided the "nano--obstruction/locking effect" in the hydrogel, and it could be applied in the drug delivery system for controlled drug release (Lin et al., 2016). TPP is an ionic cross-linker, having three phosphate groups (triple-negative charges), and it has been used as a cross-linking agent for chitosan. Since chitosan has OH and NH_2 groups, and the NH_2 are easily protonated to NH_3^+ below its pK_a, which could bind to the negative phosphate groups. It has been reported that the conventional Ch-TPP complex is a metastable system with poor mechanical and is highly pH-dependent. As the pK_a of chitosan is 6.5, thus at pH of 3.4, 5.5, and 6, 100%, 90% and 40% of amino groups were protonated, respectively (Bayat et al., 2008; Karimi et al., 2013). Additionally, Wei et al. (2020) reported that when the TPP

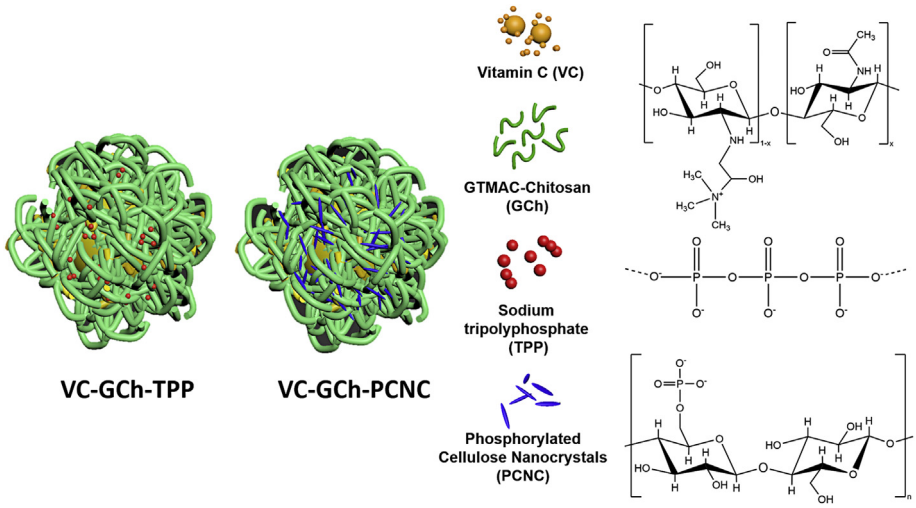

Scheme 2. Schematic illustrations describing the microstructure of the nanocapsules and the chemical functionality of each of the components.

content was lower than 0.04%, a burst release of theophylline (TH) in TH/Ch-TPP particles was observed within 2 h while at 0.04% of TPP content, 90% of TH was slowly released within 5 h (Wei et al., 2020). In comparison, our PCNC containing nanocapsules showed prolonged VC release, hence they are considered to be a better delivery system.

Fig. 1B shows the size and zeta potential of the GCh nanocapsules loaded with VC and cross-linked with TPP or PCNC. The larger particle size of 620 nm was obtained by electrostatic interaction with negatively charged VC and highly positive GCh. However, VC's high affinity towards GCh neutralized the cationic charges on the GCh, which reduced the stability of the complex and might induce the aggregation of the system (Fig.1Ca). This tendency of aggregation may be addressed using other strategies to prepare a stable nanoparticulate system. The alternative methodologies of incorporating TPP or PCNC yielded highly stable nanocapsules with zeta potential values of about −31 mV and −26 mV, respectively. Eyley and Thielemans (2014) stated that the acid hydrolysis of CNC using sulfuric or phosphoric acid imparted negative charges to the CNC from the decoration of sulfate or phosphate groups on the surface of CNC. If the phosphate groups on the CNC surface are insufficient, it has the tendency to aggregate (Eyley and Thielemans, 2014). The alternative methodologies of incorporating TPP or PCNC produced nanocapsules with zeta potentials of about −30 mV, which is considered highly stable. VC-GCh possessed a zeta potential (ZP) of ~+9 mV, which decreased to ~ −30 mV when the VC-GCh was complexed with TPP and PCNC. The average particle diameter of 450 ± 8 and 428 ± 6 nm was reported for VC-GCh-PCNC and VC-GCh-TPP nanocapsules. Consequently, both nanocapsules yielded 0.05 as the average PDI, confirming the uniform size distribution of the nanocapsules without aggregation. Wang et al. (2017) reported that anthocyanins, which are blueberry extracts, were added to form microcapsules with CNC and TPP as a cross-linking agent. The anthocyanins were distributed in the entire microcapsule, such as on the capsule surface, core, and matrix. In their prepared Ch-CNC microcapsules, anthocyanins were present in the core and the surface, whereas anthocyanins were found on the surface of the Ch-TPP microcapsules. The anthocyanins could not be encapsulated within the core due to the weaker matrix with larger pores within the matrix. Besides, the sizes of their Ch-CNC and Ch-TPP microcapsules were 265–969 nm and ~34 μm respectively (Wang et al., 2017). However, the size of Ch-TPP subjected to high-intensity ultrasonication was around 300 nm with a PDI of 0.53 (Tang et al., 2003). Fig. 1C depicts the morphology of VC-GCh (a), VC-GCh-PCNC (b) and VC-GCh-TPP (c) nanocapsules, and Scheme 2 summarizes the microstructure of the nanocapsules and the chemical functionality of each components, and the TEM images confirmed the formation of spherical and monodispersed nanocapsules. The VC-GCh mixture formed through ionic gelation possessed an amorphous structure of around 600–620 nm (Fig. 1Ca). Both VC-loaded VC-GCh-TPP (Fig. 1Cb) and VC-GCh-PCNC nanocapsules (Fig. 1Cc) maintained a spherical shape with an average size of 400–500 nm. The sample cross-linked using PCNC showed enhanced contrast signals compared to VC-GCh-TPP, associated with high VC encapsulation. Additionally, this phenomenon supported our hypothesis of better cross-linking capacity and higher VC loading in the GCh-PCNC system.

External environmental conditions, such as light, high temperatures, low pH, and dissolved oxygen, could expedite the VC degradation (Burdurlu et al., 2006; Zerdin et al., 2003). Therefore, it is essential to protect the VC to yield the desired performance for a given application. Removing dissolved oxygen in a light-protected environment is an important measure to ensure no VC degradation. As shown in Fig. 2A,

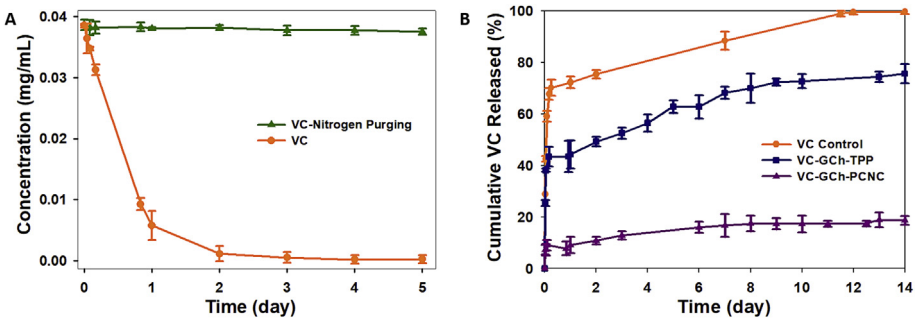

Fig. 2. (A) Changes in concentration concerning the time of a 0.04 mg/mL VC solution in PBS under nitrogen gas purging, limited light exposure, and constant temperature. **(B)** The cumulative release profile of VC from nanocapsules through a dialysis membrane to time.

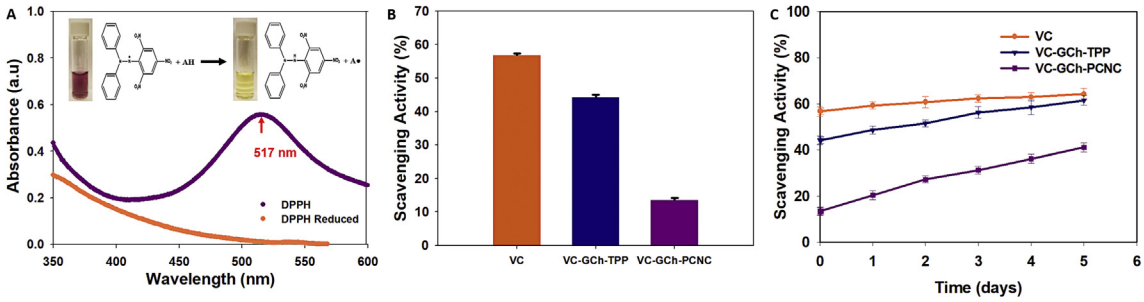

Fig. 3. (A) DPPH absorption spectra, **(B)** DPPH free radical scavenging activity from the filtrates of nanocapsule dispersions of VC- GCh-TPP and VC-GCh-PCNC for 30 min, and **(C)** DPPH free radical scavenging activity from the filtrates of nanocapsule dispersions of VC- GCh-TPP and VC-GCh-PCNC for 5 days.

nitrogen purging yielded minimal to no degradation over 5 days compared to the VC exposed to ambient conditions. Without nitrogen purging, degradation of VC occurred rapidly, where the VC degraded by 86% within the first 24 h and 100% within 4 days. Moreover, a controlled environment prevented the degradation of VC, with the concentration maintained at almost 98% at the end of 5 days. Thus, the optimal condition for conducting the VC release required continuous nitrogen purging, which was being adopted for the accurate VC quantification from the prepared nanocapsules.

The encapsulation efficiency for both VC-GCh-PCNC and VC-GCh-TPP nanocapsules were measured in neutral pH. Since the pK_a of vitamin C is pH 4.2 and 11.6 (Tian et al., 2009), the vitamin C was partially ionized at neutral pH, yielding negative charges that would bind to GCh, resulting in a higher encapsulation of VC. The indirect method yielded an EE of 90.3 ± 0.42% for VC-GCh-PCNC, which was 33% higher than VC-GCh-TPP (57.3 ± 0.28%) nanocapsules. This significant difference in EE confirmed that nanocapsules prepared using GCh and PCNC possessed good encapsulation of VC and stability due to the chemical bonding compared to the weaker TPP cross-linked VC-GCh-TPP nanocapsule system. In the previous study by Desai and co-workers, the encapsulation efficiency of VC loaded Ch-TPP capsules using different molecular weight types were between 52.74 and 67.25% (Desai et al., 2006).

An incremental release test to simulate food storage performed over 14 days under continuous nitrogen purging conditions is shown in Fig. 2B. A burst release of more than 75% in the first few hours was observed for VC only (control) compared to 40% for VC-GCh-TPP and 10% for VC-GCh-PCNC, thereby confirming the importance of encapsulation. We observed that the VC-GCh-TPP nanocapsules displayed a more rapid release profile of 42% within a day and approached 76% within two weeks. In contrast, VC-GCh-PCNC showed a slow-release of VC, approaching about 18% over the extended period of 14 days. A slow release of VC was achieved using VC-GCh-PCNC, since the PCNC possessed a more robust and a durable cross-links with GCh compared to TPP. Water-soluble GCh crosslinked using TPP has been reported for encapsulating protein, insulin, quercetin, and Bovine Serum Albumin (BSA) (Rwei et al., 2014; Zhang et al., 2010), and an initial burst coupled with a slow/continuous release were observed in an *in-vitro* study. Despite the high EE% and slow release rate of GCh-TPP compared to Ch-TPP, almost 72–80% were released within 24 h due to the weak ionization degree of GCh at pH 7.4 and fewer positively charged groups. However, in our study, PCNC functioned as a filler for the GCh matrix (Xu et al., 2019), thereby improving the mechanical strength of the nanocapsules that contributed to the controlled release of VC. Therefore, the VC-GCh-PCNC would be more useful for the long-term storage of active ingredients in foods, cosmetics, and personal care applications.

The DPPH solution is violet in color and has a characteristic UV–visible absorption peak at 517 nm in the non-reduced state (Fig. 3A). The results of the DPPH free radical scavenging activity experiments for VC, VC-GCh-TPP, and VC-GCh-PCNC nanocapsules for 30 min are shown in Fig. 3B. A higher scavenging activity in the filtrate (free VC) corresponded to a lower encapsulating capacity of the nanocapsules and vice versa. As seen in Fig. 3B, the filtrate of VC-GCh-PCNC possessed a low scavenging activity of 13.5 ± 0.58% compared to VC-GCh-TPP (44.7 ± 0.89%) and free VC (56.7 ± 0.62%) after 30 min. Fig. 3C shows the antioxidant power over 5 days, displaying still lower scavenging activity (%) for the VC-GCh-PCNC. However, in contrast, the retained VC in GCh-PCNC nanocapsules possessed a significant free-radical scavenging activity than VC in GCh-TPP. Since PCNC provided a better cross-linking capacity with GCh yielding a compact nanocapsule that preserved the VC from external degradation over a long storage time.

Table 2
Rate and correlation constants for both VC-GCh-PCNC and VC-GCh-TPP nanocapsules fit zero-order, first-order, and Higuchi mathematical models.

Nanocapsule	Zero-Order		First-Order		Higuchi	
	K_0 (h^{-1})	R^2	K_1 (h^{-1})	R^2	K_H ($h^{0.5}$)	R^2
VC-GCh-PCNC	0.05	0.92	3×10^{-4}	0.97	0.77	0.96
VC-GCh-TPP	0.17	0.91	1.7×10^{-3}	0.97	2.79	0.95

The data obtained from the VC release studies from VC-GCh-PCNC and VC-GCh-TPP nanocapsules were used to elucidate the various drug release kinetic models (Zero-Order, First-Order, and Higuchi). The zero-order release corresponds to a constant release with the same amount of VC release per unit time. The first-order model is a concentration-dependent release with the same rate of drug release per unit time, and corresponded to a sustained-release and matrix diffusion-controlled release. The Higuchi model can be used to determine the release of the drug from the matrix (Fu and Kao, 2010; Mircioiu et al., 2019). Based on equations (3-5), the best kinetic model was determined by the highest coefficients of determination (R^2). These kinetic equations offer insights into the VC release mechanism, and delivery behaviour from nanocapsules. Besides, the rate constants (k) were obtained from the linear regressions of these models (Table 2), and they were used to identify the best model for the release of VC from the nanocapsules. Both first-order and Higuchi models yielded sufficiently high correlation constants (>0.95), indicating a good fit for the kinetic data. A first-order fit suggests that the release of VC from the nanocapsules corresponded to the sustained-release and matrix diffusion-controlled release. In contrast, a good fit to the Higuchi model represented a diffusing water-soluble drug in a matrix system, where the square root of time-dependent release is associated with the Fickian diffusion (Caccavo et al., 2015; Chiarappa et al., 2017). In summary, the VC release was mediated by diffusion from the GCh matrix, where the VC was electrostatically bound. The diffusion rate was attributed to the GCh-PCNC polymer matrix's strength due to cross-linking resulting in the lowest VC release. It was evident from Table 2 that the kinetic constants of VC-GCh-PCNC were 3–4 times lower than VC-GCh-TPP, which further confirmed that PCNC was a better cross-linking agent.

* K_0 is the zero-order release constant.
* K_1 is the first-order release constant.

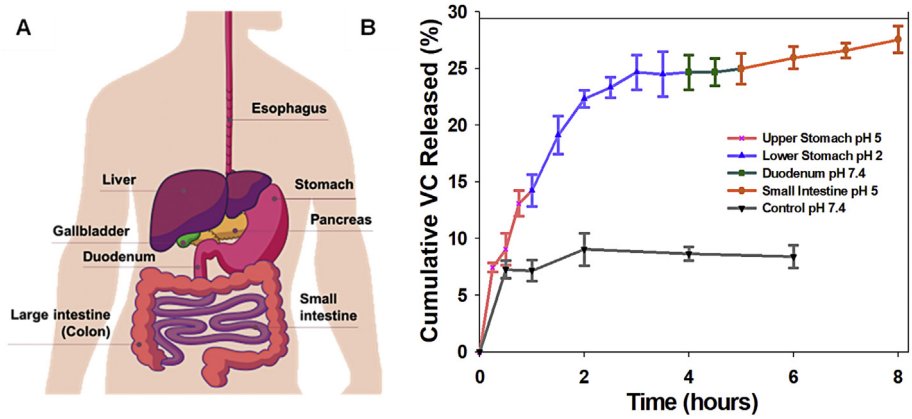

Fig. 4. (A): diagram of human digestive system and (B): *In vitro* simulation of various conditions of the digestive system of VC-GCh-PCNC.

* K_H is the Higuchi dissolution constant.

Theoretically, as depicted in Fig. 4A, orally swallowed food passes through the esophagus to reach the stomach in several seconds. The food remains in the stomach and is digested by the gastric acid and enzymes (pH 1–3, 1.5–4 h), after which it enters the duodenum, and the small intestine via peristalsis, induced by a series of muscular contractions. It is mixed with digestive juices and enzymes from the pancreas, liver, and intestine (pH 6–8, 1–2 h), where the water and nutrients are absorbed into the bloodstream. As peristalsis continues, the food and fluid movement's conveyed the undigested fractions to the large intestine (pH 5–7, 12–24 h) where the remaining water is absorbed, resulting in the solid stool (McClements and Li, 2010). The digestion of VC occurs similarly, and after ingestion, it will be oxidized to DHA and absorbed in the small intestine (Akyön, 2002). The release profiles of VC-GCh-PCNC in a simulated human digestive system at the specific pH environments and pH 7.4 (control) are shown in Fig. 4B. When changing the release medium pH to simulate the conditions of the digestive system, it was observed that a higher cumulative VC release over 8 h was observed compared to the release at the control pH of 7.4. At 8 h, the digestion simulation had achieved a release of approximately 27%, compared to neutral pH, where less than 10% of the VC was released. Since chitosan and CNC possess mucoadhesive property, they could attach to the mucous membrane and slowly release the VC. Cationic chitosan exhibited high mucoadhesive properties and could bind to negatively charged mucin, resulting in a strong mucosal adhesion. Moreover, the high surface area could interact with mucin rather than Tempo-CNF and CNF, and hydrophobic attraction or hydrogen bonding promotes the adhesion of mucin to CNC (Lin et al., 2019). After digestion, chitosan could be degraded by enzymes, such as lysozyme and human bacterial enzymes in our body fluid especially in our lungs and colons. Lončarević et al. stated that in the enzymatic digestion process, the enzyme first diffuses to the solution and partitions to the surface of the complex. The enzyme on the complex initiates the catalytic reaction that results in the scission of the macromolecular backbone, and the bioactive substance is then released into the bulk solution (Lončarević et al., 2017). If the chitosan complex is porous, then the degradation would occur more rapidly. Hence with the addition of CNC, which acted as a reinforcement in the chitosan complex, the degradation and burst releasing were significantly reduced. However, as there is a lack of cellulase intake by the human body, most of the CNC will be excreted, or it could be fermented by gut microflora, such as Ruminococcus champanellensis present in the human fecal (Zhang et al., 2018). The pH sensitivity of the nanocapsules is desirable in food preparations to ensure that VC remains encapsulated and protected during storage, whereby in the digestive tract following ingestion, a controlled release is desirable.

It is well-known that chitosan possesses antibacterial properties against a wide range of microorganisms. The antimicrobial characteristic of chitosan is affected by intrinsic and extrinsic factors, such as strain, pH, ionic strength, molecular weight or degree of deacetylation of chitosan etc. Chitosan loses its antimicrobial function above its pK_a due to the deprotonation of the amino groups and its low solubility in water. However, Atay (2019) claimed that chitosan has limited activity because amino groups in chitosan backbone can only act as weak positive charge center (Atay, 2019). Therefore, in this study, we enhanced the antibacterial property by grafting GTMAC to the chitosan backbone to introduce more cationic groups to the chitosan that will bind to the negative cell membrane and kill the bacteria. The range of antimicrobial activities of GCh against *E. coli* and *S. aureus* was 16–32 μg/mL and 8–16 μg/mL, respectively (Fig. 5). Other reasons for the antimicrobial effects of the complex are: VC has been shown to possess antibacterial property against *S. epidermidis, E. coli and P. aeruginosa* (Pandit et al., 2017) and low concentration of VC (0.15 mg/mL) inhibited the growth of *S. aureus* (Mousavi et al., 2019). Liping et al. (2020) developed water-soluble

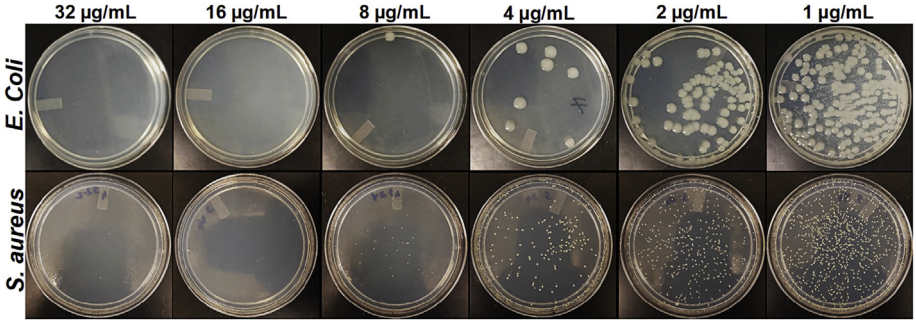

Fig. 5. Antimicrobial activity of VC- GCh-PCNC with *E. coli* and with *S. aureus*. (*MIC values of GTMAC-Chitosan for two types of bacteria were 32–64 μg/mL-data not shown).

chitosan with vitamin C complex (CSVC) and confirmed its antibacterial activity against *E. coli*. Compared to the blank control, the MIC of CSVC against *E. coli* was about 5 mg/mL (Liping et al., 2020). In this study, due to the quaternary ammonium groups and the presence of VC, the nanocapsule system inhibited the pathogenic bacteria population at minimal concentrations. Thus, VC-GCh-PCNC could reduce bacteria contamination over a reasonably long period, making them a suitable antimicrobial agent for functional food systems.

4. Conclusions

This study examines the stabilization mechanism and effectiveness of PCNC over TPP on improving the stability, encapsulation, and VC release in the VC-GCh-PCNC nanocapsule system. PCNC could effectively stabilize the system via stronger ionic gelation compared to TPP. The stability of VC in the system is highly dependent on light, pH, and dissolved oxygen of the environment. A better kinetic release of VC was achieved under nitrogen purge. The PCNC cross-linked nanocapsules possessed a sustained release profile, making them ideal candidates for prolonged VC storage. The kinetic release profiles were fitted to the first-order and Higuchi kinetic models ($R^2 > 0.95$), showing a concentration-dependent release from the VC-GCh-PCNC nanocapsule system. A digestive system simulated *in vitro* release tests by varying the pHs, which showed a faster release rate at low pHs that was attributed to the degree of quaternization of GCh. The sedimented VC-GCh-PCNC possessed a higher antioxidant capacity than VC-GCh-TPP. Additionally, the MIC for *E. coli* and *S. aureus* bacterial strains were between 8 and 16 μg/mL, which suggested that the VC-GCh-PCNC nanocapsules were efficient antimicrobial agents that could extend the shelf-life of food systems . These results showed that the VC's stability was enhanced in the presence of PCNC, thereby offering a strategy for the preservation of highly unstable compounds (such as VC) during long-term storage in functional food systems.

Funding

Professor K. C. Tam wishes to acknowledge the funding from CFI and NSERC.

CRediT authorship contribution statement

Jiyoo Baek: Conceptualization, Methodology, Data curation, Investigation, Writing – original draft. **Mohankandhasamy Ramasamy:** Writing – review & editing, Software, Supervision. **Natasha Carly Willis:** Writing – original draft, Formal analysis, Investigation. **Dae Sung Kim:** Formal analysis. **William A. Anderson:** Resources, Validation. **Kam C. Tam:** Funding acquisition, Resources, Visualization, Validation, Writing – review & editing, Supervision.

Declaration of competing interest

The authors declare that they have no known competing financial interests or personal relationships that could have appeared to influence the work reported in this paper.

Acknowledgements

CelluForce and AboraNano supported this CNC based research.

References

Akhlaghi, S.P., Berry, R.M., Tam, K.C., 2015. Modified cellulose nanocrystal for vitamin C delivery. AAPS PharmSciTech 16 (2), 306–314.
Akyön, Y., 2002. Effect of antioxidants on the immune response of Helicobacter pylori. Clin. Microbiol. Infect. 8 (7), 438–441.
Alishahi, A., Mirvaghefi, A., Tehrani, M.R., Farahmand, H., Shojaosadati, S.A., Dorkoosh, F.A., Elsabee, M.Z., 2011. Shelf life and delivery enhancement of vitamin C using chitosan nanoparticles. Food Chem. 126 (3), 935–940.
Ashrafizadeh, M., Tam, K.C., Javadi, A., Abdollahi, M., Sadeghnejad, S., Bahramian, A., 2020. Dual physically and chemically cross-linked polyelectrolyte nanohydrogels: compositional and pH-dependent behavior studies. Eur. Polym. J. 122, 109398.
Atay, H.Y., 2019. Antibacterial activity of chitosan-based systems. In: Functional Chitosan. Springer, pp. 457–489.
Azevedo, M.A., Bourbon, A.I., Vicente, A.A., Cerqueira, M.A., 2014. Alginate/chitosan nanoparticles for encapsulation and controlled release of vitamin B2. Int. J. Biol. Macromol. 71, 141–146.
Baek, J., Wahid-Pedro, F., Kim, K., Kim, K., Tam, K.C., 2019. Phosphorylated-CNC/modified-chitosan nanocomplexes for the stabilization of Pickering emulsions. Carbohydr. Polym. 206, 520–527.
Bayat, A., Dorkoosh, F.A., Dehpour, A.R., Moezi, L., Larijani, B., Junginger, H.E., Rafiee-Tehrani, M., 2008. Nanoparticles of quaternized chitosan derivatives as a carrier for colon delivery of insulin: ex vivo and in vivo studies. Int. J. Pharm. 356 (1–2), 259–266.
Bendich, A., Machlin, L., Scandurra, O., Burton, G., Wayner, D., 1986. The antioxidant role of vitamin C. Adv. Free Radic. Biol. Med. 2 (2), 419–444.
Bodannes, R.S., Chan, P.C., 1979. Ascorbic-acid as a scavenger of singlet oxygen. FEBS Lett. 105 (2), 195–196.
Burdurlu, H.S., Koca, N., Karadeniz, F., 2006. Degradation of vitamin C in citrus juice concentrates during storage. J. Food Eng. 74 (2), 211–216.
Caccavo, D., Cascone, S., Lamberti, G., Barba, A.A., 2015. Controlled drug release from hydrogel-based matrices: experiments and modeling. Int. J. Pharm. 486 (1–2), 144–152.
Chiarappa, G., Abrami, M., Dapas, B., Farra, R., Trebez, F., Musiani, F., Grassi, G., Grassi, M., 2017. Mathematical modeling of drug release from natural polysaccharides based matrices. Natural Product Communications 12 (6), 873–880.
de Britto, D., de Moura, M.R., Aouada, F.A., Mattoso, L.H., Assis, O.B., 2012. N, N, N-trimethyl chitosan nanoparticles as a vitamin carrier system. Food Hydrocolloids 27 (2), 487–493.
Desai, K., Park, H.J., 2005. Encapsulation of vitamin C in tripolyphosphate cross-linked chitosan microspheres by spray drying. J. Microencapsul. 22 (2), 179–192.
Desai, K., Liu, C., Park, H.J., 2006. Characteristics of vitamin C encapsulated tripolyphosphate-chitosan microspheres as affected by chitosan molecular weight. J. Microencapsul. 23 (1), 79–90.
Deshpande, S., 2002. Handbook of Food Toxicology. CRC Press, New York- Basel.
Espinosa, S.C., Kuhnt, T., Foster, E.J., Weder, C., 2013. Isolation of thermally stable cellulose nanocrystals by phosphoric acid hydrolysis. Biomacromolecules 14 (4), 1223–1230.
Eyley, S., Thielemans, W., 2014. Surface modification of cellulose nanocrystals. Nanoscale 6 (14), 7764–7779.
Fu, Y., Kao, W.J., 2010. Drug release kinetics and transport mechanisms of non-degradable and degradable polymeric delivery systems. Expet Opin. Drug Deliv. 7 (4), 429–444.
Geng, C.-z., Hu, X., Yang, G.-h., Zhang, Q., Chen, F., Fu, Q., 2015. Mechanically reinforced chitosan/cellulose nanocrystals composites with good transparency and biocompatibility. Chin. J. Polym. Sci. 33 (1), 61–69.
He, G., Kong, Y., Zheng, H., Ke, W., Chen, X., Yin, Y., Yi, Y., 2018. Preparation and properties of poly (amidoamine) dendrimer/quaternary ammonium chitosan hydrogels. J. Wuhan Univ. Technol.-Materials Sci. Ed. 33 (3), 736–743.
Jiménez-Fernández, E., Ruyra, A., Roher, N., Zuasti, E., Infante, C., Fernández-Díaz, C., 2014. Nanoparticles as a novel delivery system for vitamin C administration in aquaculture. Aquaculture 432, 426–433.
Karimi, M., Avci, P., Ahi, M., Gazori, T., Hamblin, M.R., Naderi-Manesh, H., 2013. Evaluation of chitosan-tripolyphosphate nanoparticles as a p-shRNA delivery vector: formulation, optimization and cellular uptake study. Journal of nanopharmaceutics and drug delivery 1 (3), 266–278.
Katouzian, I., Jafari, S.M., 2016. Nano-encapsulation as a promising approach for targeted delivery and controlled release of vitamins. Trends Food Sci. Technol. 53, 34–48.
Kumar, M.N.V.R., 2000. A review of chitin and chitosan applications. React. Funct. Polym. 46 (1), 1–27.
Larsen, S.W., Ostergaard, J., Yaghmur, A., Jensen, H., Larsen, C., 2013. Use of in vitro release models in the design of sustained and localized drug delivery systems for subcutaneous and intra-articular administration. J. Drug Deliv. Sci. Technol. 23 (4), 315–324.
Lazaridou, M., Christodoulou, E., Nerantzaki, M., Kostoglou, M., Lambropoulou, D.A., Katsarou, A., Pantopoulos, K., Bikiaris, D.N., 2020. Formulation and in-vitro characterization of chitosan-nanoparticles loaded with the iron chelator deferoxamine mesylate (DFO). Pharmaceutics 12 (3), 238.
Li, C., Yu, W., Wu, P., Chen, X.D., 2020. Current in vitro digestion systems for understanding food digestion in human upper gastrointestinal tract. Trends Food Sci. Technol. 96, 114–126.
Lim, S.-H., Hudson, S.M., 2003. Review of chitosan and its derivatives as antimicrobial agents and their uses as textile chemicals. J. Macromol. Sci. Polym. Rev. 43 (2), 223–269.
Lin, N., Gèze, A., Wouessidjewe, D., Huang, J., Dufresne, A., 2016. Biocompatible double-membrane hydrogels from cationic cellulose nanocrystals and anionic alginate as complexing drugs codelivery. ACS Appl. Mater. Interfaces 8 (11), 6880–6889.
Lin, Y.-J., Shatkin, J.A., Kong, F., 2019. Evaluating mucoadhesion properties of three types of nanocellulose in the gastrointestinal tract in vitro and ex vivo. Carbohydr. Polym. 210, 157–166.

Liping, L., Kexin, L., Huipu, D., Jia, L., Jie, Z., 2020. Study on preparation of a chitosan/vitamin C complex and its properties in cosmetics. Natural Product Communications 15 (10), 1934578X20946876.
Liu, J., Li, H., Chen, D., Jin, X., Zhao, X., Zhang, C., Ping, Q., 2011. In vivo evaluation of novel chitosan graft polymeric micelles for delivery of paclitaxel. Drug Deliv. 18 (3), 181–189.
Lončarević, A., Ivanković, M., Rogina, A., 2017. Lysozyme-induced degradation of chitosan: the characterisation of degraded chitosan scaffolds. Journal of Tissue Repair and Regeneration 1 (1), 12.
Loutfy, S.A., El-Din, H.M.A., Elberry, M.H., Allam, N.G., Hasanin, M., Abdellah, A.M., 2016. Synthesis, characterization and cytotoxic evaluation of chitosan nanoparticles: in vitro liver cancer model. Adv. Nat. Sci. Nanosci. Nanotechnol. 7 (3), 035008.
Martins, A.F., de Oliveira, D.M., Pereira, A.G., Rubira, A.F., Muniz, E.C., 2012. Chitosan/TPP microparticles obtained by microemulsion method applied in controlled release of heparin. Int. J. Biol. Macromol. 51 (5), 1127–1133.
McClements, D.J., Li, Y., 2010. Structured emulsion-based delivery systems: controlling the digestion and release of lipophilic food components. Adv. Colloid Interface Sci. 159 (2), 213–228.
Mircioiu, C., Voicu, V., Anuta, V., Tudose, A., Celia, C., Paolino, D., Fresta, M., Sandulovici, R., Mircioiu, I., 2019. Mathematical modeling of release kinetics from supramolecular drug delivery systems. Pharmaceutics 11 (3), 140.
Mousavi, S., Bereswill, S., Heimesaat, M.M., 2019. Immunomodulatory and antimicrobial effects of vitamin C. European Journal of Microbiology and Immunology 9 (3), 73–79.
Naidu, K.A., 2003. Vitamin C in human health and disease is still a mystery? An overview. Nutr. J. 2 (1), 7.
Pandit, S., Ravikumar, V., Abdel-Haleem, A.M., Derouiche, A., Mokkapati, V., Sihlbom, C., Mineta, K., Gojobori, T., Gao, X., Westerlund, F., Mijakovic, I., 2017. Low concentrations of vitamin C reduce the synthesis of extracellular polymers and destabilize bacterial biofilms. Front. Microbiol. 8, 2599.
Radtchenko, I.L., Sukhorukov, G.B., Möhwald, H., 2002. Incorporation of macromolecules into polyelectrolyte micro-and nanocapsules via surface controlled precipitation on colloidal particles. Colloid. Surface. Physicochem. Eng. Aspect. 202 (2–3), 127–133.
Rinaudo, M., 2006. Chitin and chitosan: properties and applications. Prog. Polym. Sci. 31 (7), 603–632.
Rosenzweig, O., Lavy, E., Gati, I., Kohen, R., Friedman, M., 2013. Development and in vitro characterization of floating sustained-release drug delivery systems of polyphenols. Drug Deliv. 20 (3–4), 180–189.
Rwei, S.-P., Chen, Y.M., Lin, W.Y., Chiang, W.Y., 2014. Synthesis and rheological characterization of water-soluble glycidyltrimethylammonium-chitosan. Mar. Drugs 12 (11), 5547–5562.
Sampath, U.T.M., Ching, Y.C., Chuah, C.H., Singh, R., Lin, P.C., 2017. Preparation and characterization of nanocellulose reinforced semi-interpenetrating polymer network of chitosan hydrogel. Cellulose 24 (5), 2215–2228.
Sauberlich, H.E., 1994. Pharmacology of vitamin C. Annu. Rev. Nutr. 14 (1), 371–391.
Shi, Z.Q., Tang, J.T., Chen, L., Yan, C.R., Tanvir, S., Anderson, W.A., Berry, R.M., Tam, K.C., 2015. Enhanced colloidal stability and antibacterial performance of silver nanoparticles/cellulose nanocrystal hybrids. J. Mater. Chem. B 3 (4), 603–611.
Siepmann, J., Siepmann, F., 2013. Mathematical modeling of drug dissolution. Int. J. Pharm. 453 (1), 12–24.
Simpson, G.L.W., Ortwerth, B.J., 2000. The non-oxidative degradation of ascorbic acid at physiological conditions. Biochim. Biophys. Acta (BBA) - Mol. Basis Dis. 1501 (1), 12–24.
Starychova, L., Zabka, M., Spaglova, M., Cuchorova, M., Vitkova, M., Cierna, M., Bartoníková, K., Gardavska, K., 2014. In vitro liberation of indomethacin from chitosan gels containing microemulsion in different dissolution mediums. J. Pharmaceut. Sci. 103 (12), 3977–3984.
Tang, E., Huang, M., Lim, L.Y., 2003. Ultrasonication of chitosan and chitosan nanoparticles. Int. J. Pharm. 265 (1–2), 103–114.
Tian, X., Tian, D., Wang, Z., Mo, F., 2009. Synthesis and evaluation of chitosan-vitamin C complex. Indian J. Pharmaceut. Sci. 71 (4), 371.
Vanderfleet, O.M., Osorio, D.A., Cranston, E.D., 2018. Optimization of cellulose nanocrystal length and surface charge density through phosphoric acid hydrolysis. Phil. Trans. Math. Phys. Eng. Sci. 376 (2112).
Wang, W.J., Jung, J., Zhao, Y.Y., 2017. Chitosan-cellulose nanocrystal microencapsulation to improve encapsulation efficiency and stability of entrapped fruit anthocyanins. Carbohydr. Polym. 157, 1246–1253.
Wei, Y., Huang, Y.-H., Cheng, K.-C., Song, Y.-L., 2020. Investigations of the influences of processing conditions on the properties of spray dried chitosan-tripolyphosphate particles loaded with theophylline. Sci. Rep. 10 (1), 1–12.
Xu, Q., Ji, Y., Sun, Q., Fu, Y., Xu, Y., Jin, L., 2019. Fabrication of cellulose nanocrystal/chitosan hydrogel for controlled drug release. Nanomaterials 9 (2), 253.
Xu, X., Liu, Y., Fu, W., Yao, M., Ding, Z., Xuan, J., Li, D.X., Wang, S.J., Xia, Y.Q., Cao, M., 2020. Poly (N-isopropylacrylamide)-based thermoresponsive composite hydrogels for biomedical applications. Polymers 12 (3), 580.
Zandi, M., 2017. Evaluation of the kinetics of ascorbic acid (aa) release from alginate-whey protein concentrates (Al-wpc) microspheres at the simulated gastrointestinal condition. J. Food Process. Eng. 40 (1).
Zerdin, K., Rooney, M.L., Vermue, J., 2003. The vitamin C content of orange juice packed in an oxygen scavenger material. Food Chem. 82 (3), 387–395.
Zhang, H.-l., Wu, S.-h., Tao, Y., Zang, L.-q., Su, Z.Q., 2010. Preparation and characterization of water-soluble chitosan nanoparticles as protein delivery system. J. Nanomater. 2010, 898910 https://doi.org/10.1155/2010/898910, 5 pages.
Zhang, T., Yang, Y., Liang, Y., Jiao, X., Zhao, C., 2018. Beneficial effect of intestinal fermentation of natural polysaccharides. Nutrients 10 (8), 1055.